communications physics

Article

https://doi.org/10.1038/s42005-025-01976-8

Deconfined quantum critical point lost in pressurized $SrCu_2(BO_3)_2$

Jing Guo [1,6], Pengyu Wang[1,2,6], Cheng Huang [3,6], Bin-Bin Chen [3], Wenshan Hong [1,2], Shu Cai[1,4], Jinyu Zhao [1,2], Jinyu Han[1,2], Xintian Chen[1,2], Yazhou Zhou[1], Shiliang Li [1,2,5], Qi Wu[1], Zi Yang Meng [3] ✉ & Liling Sun [1,2,4] ✉

The deconfinement quantum critical point (DQCP), a paradigm beyond the Landau-Ginzburg-Wilson framework to classify states of matters, has been attracting extensive attention over the past two decades. Experimentally, $SrCu_2(BO_3)_2$ plays key roles in verifying the DQCP between an antiferromagnetic (AF) Néel phase and a plaquette-singlet (PS) phase. However, the verification of the DQCP of the PS-AF transition lies in 2.4 - 3.1 GPa, which is unreachable previously due to technical limitations. Here, through the advanced high-pressure heat capacity measurements, we demonstrate that the PS-AF phase transition of $SrCu_2(BO_3)_2$ at zero field is clearly first-order. Our result clarifies the two-decade-long debates about this key issue and resonates nicely with recent theoretical consensus that the previously predicted DQCPs in representative models are actually first-order transitions. Besides, the PS and AF phases transit at the same pressure-temperature point, a bi-critical point found in frustrated magnets.

The deconfined quantum critical point (DQCP) is a concept to describe the continuous phase transition between two different spontaneous symmetry-breaking phases in correlated materials at zero temperature[1,2]. It is characterized by the absence of confinement, i.e., the state of elementary excitations carries fractionalized quantum number and interacts via emergent gauge field—different from those as predicted by the conventional phase transitions[3–5]. The concept of the DQCP attracts widespread attention because it gives rise to exotic states of matters, along with the Berezinskii-Kosterlitz-Thouless (BKT) transition[6,7], anyon condensations[8,9] and those in topological insulators and high-temperature superconductors, challenging the conventional understanding of matter within the paradigm of Landau-Ginzberg-Wilson (LGW) where symmetries and their spontaneous breaking are the dominated factors. Fractionalization and emergent gauge fields of DQCP also have potential applications in quantum computing and quantum information.

In the past two decades, investigations on DQCP have been active, as enormous efforts have been made to explore various theoretical models and experimental systems to realize the DQCP and its associated consequences[10–23]. However, a key question about whether the proposed DQCP models really host a continuous phase transition corresponding to a true conformal field theory (CFT) remains controversial. Previous results suggest that the DQCP is realized in some 2D quantum spin or interacting Dirac fermion lattice models[10,22] and the transition of two different spontaneous symmetry-breaking phases appears to be continuous, but the finite-size scaling is not consistent with regular scaling ansatz[13,15,23], and the extracted scaling dimensions are incompatible with later evaluations based on conformal bootstrap[24]. The controversy is more clearly revealed very recently that the DQCP "fails" a series of general standards from a quantum entanglement perspective that all CFTs are expected to meet[25–36], and further theoretical developments find that previously predicted DQCPs in representative spin lattice models are weakly first-order transitions[28–34]. Such recent consensus seems to conclude the nature of the Neel-to-VBS transition in the spin DQCP model after two decades of debating.

At the experimental frontier, material realizations and detections of the DQCP are equally active. Among quantum magnets, the layered material, $SrCu_2(BO_3)_2$, is an ideal candidate for realizing DQCP due to its unique crystal structure[37–46]. As shown in Fig. 1a, b, Cu^{2+} ions (in $3d^9$ configuration) in monolayer $SrCu_2(BO_3)_2$ form a dimerized singlets (DS) state at ambient pressure, which couples the Cu^{2+} with a strong intradimer antiferromagnetic coupling J' and a weaker interdimer coupling J. The 2D network of the Cu^{2+} ions resembles the famous Shastry-Sutherland (SS) lattice[47], as shown in Fig. 1b. Application of pressure (P) can change the lattice constants of the material and consequently alter J' and J''. Previous works established the empirical relations of $J'(P) = (75 - 8.3P)$ K and $J(P) = (46.7 - 3.7P)$ K, with P being in GPa, basing on the data of high-pressure heat-capacity measurements[38,39]. By applying hydrostatic pressure

[1]Beijing National Laboratory for Condensed Matter Physics and Institute of Physics, Chinese Academy of Sciences, Beijing, China. [2]University of Chinese Academy of Sciences, Beijing, China. [3]Department of Physics and HK Institute of Quantum Science & Technology, The University of Hong Kong, Pokfulam Road, Hong Kong SAR, China. [4]Center for High Pressure Science & Technology Advanced Research, Beijing, China. [5]Songshan Lake Materials Laboratory, Dongguan, Guangdong, China. [6]These authors contributed equally: Jing Guo, Pengyu Wang, Cheng Huang. ✉e-mail: zymeng@hku.hk; llsun@iphy.ac.cn; liling.sun@hpstar.ac.cn

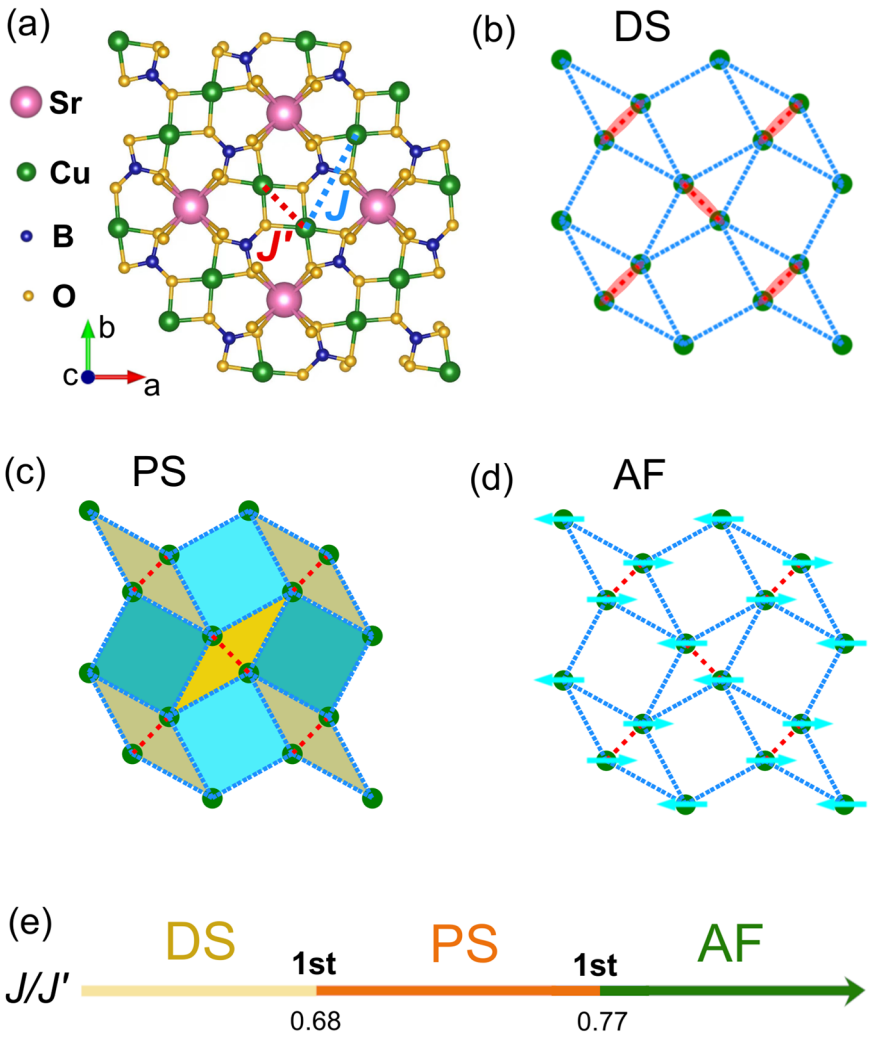

Fig. 1 | $SrCu_2(BO_3)_2$ structure, Shastry-Sutherland lattice, and the related ground-state phase diagrams. a Single layer of $SrCu_2(BO_3)_2$, where the intradimer Cu^{2+}-Cu^{2+} interaction is labeled by J' while the interdimer interaction by J. **b** Dimerized singlet (DS) state formed by Cu^{2+} in $SrCu_2(BO_3)_2$, in which J' is stronger than J at ambient pressure. The lattice is also the Shatry-Sutherland lattice. **c**, **d** The emerging states, PS and AF as J/J' increases. Note that in the PS phase, only polygons with one of the four colors, yellow, beige, teal, and cyan, form singlets and break the translational symmetry of the SS lattice. In the AF phase, the on-site spin rotational symmetry is broken. **e** Phase diagram of SS model by exact diagonalization and density matrix renormalization group calculations[42,48], where the transitions are all first-order.

above 1.8 GPa, $SrCu_2(BO_3)_2$ enters a plaquette-singlet valence bond state (VBS) (one of the four colors in Fig. 1c). Upon further increasing the pressure to above 3.1 GPa, the system transforms to an AF state[38] (Fig. 1d). However, due to technical limitations in the practical high-pressure measurements, the most important information about the nature of the PS to AF transition, which lies in the unreachable pressure range of 2.4–3.1 GPa, remains unknown.

Recent experimental works show that the application of a magnetic field perpendicular to the *ab*-plane can also trigger the transition of the $SrCu_2(BO_3)_2$ from the PS phase to the AF phase when subjecting pressure in the PS phase[39,40], exhibiting proximate critical yet first-order features. It was hypothesized that this weak first-order transition could eventually connect to a true DQCP or even a quantum spin liquid (QSL) phase close to or along the pressure axis[40]. However, recent theoretical developments have pointed out that at zero-field, the Néel-to-VBS transition in the DQCP spin model is a first-order one[25–34]. In this sense, these previous experimental works are preparational in that they have identified the two spontaneous symmetry-breaking phases (PS and Néel), and have set the stage for the conclusive answer of how these two phases transit. If the transition is continuous, then the DQCP is verified, and the paradigm beyond Landau is established. However, if the transition is first-order, then Landau is still right after all these years. We provide a conclusive answer in this work.

Results and discussion

High-pressure thermodynamics

To clarify this key puzzling issue of whether the PS-AF transition at zero field is a beyond-LGW DQCP or an LGW-allowed first-order transition experimentally (see the theoretical counterpart of the SS model in Fig. 1e) and to shine light on the overall ground-state phase diagram of the spin-1/2 SS model[42,48–53], and further to clarify whether $SrCu_2(BO_3)_2$ host an intermediate QSL phase between the AF and PS phases[54–56], in this work, we perform high-pressure heat-capacity measurements using an advanced technique, which allows us to measure the sample in a hydrostatic pressure environment with the pressure continuously tuned to above 3.1 GPa and the temperature down to 0.4 K. In particular, our redesigned high-pressure cell possesses a bigger sample chamber, which enables the load of a larger sample and provides a better pressure environment. Significantly, our redesigned high-pressure cell can reach pressures up to 3.1 GPa, exceeding the 2.5 GPa limit of commercial piston-cylinder high-pressure cells (the details can be found in Methods, Supplementary Method 1 and Fig. 1, Supplementary Method 2 and Fig. 2). We focus our measurements in the pressure range of 2.4- 3.1 GPa, and show that the PS-AF phase transition of $SrCu_2(BO_3)_2$ at zero field is clearly first-order. Our result clarifies the two-decade-long debates about this key issue and resonates nicely with the recent theoretical consensus that the previously predicted DQCPs in representative lattice models are actually first-order transitions.

As shown in Fig. 2 (Supplementary Data 1), the plots of the temperature dependence of heat capacity versus temperature (C/T) display a hump below 1.8 GPa as the temperature is reduced (Fig. 2a, b), the maximum of which is associated with the formation temperature (T_{DS}) of the dimer singlet phase from paramagnetic (PM) phase[41–43,45,46]. Upon increasing pressure to 2.1 GPa, there are two peaks appearing at low temperatures. The high-temperature one is related to the onset transition temperature from the PM phase to the PS liquid (PSL) state (T_{PSL}), and the

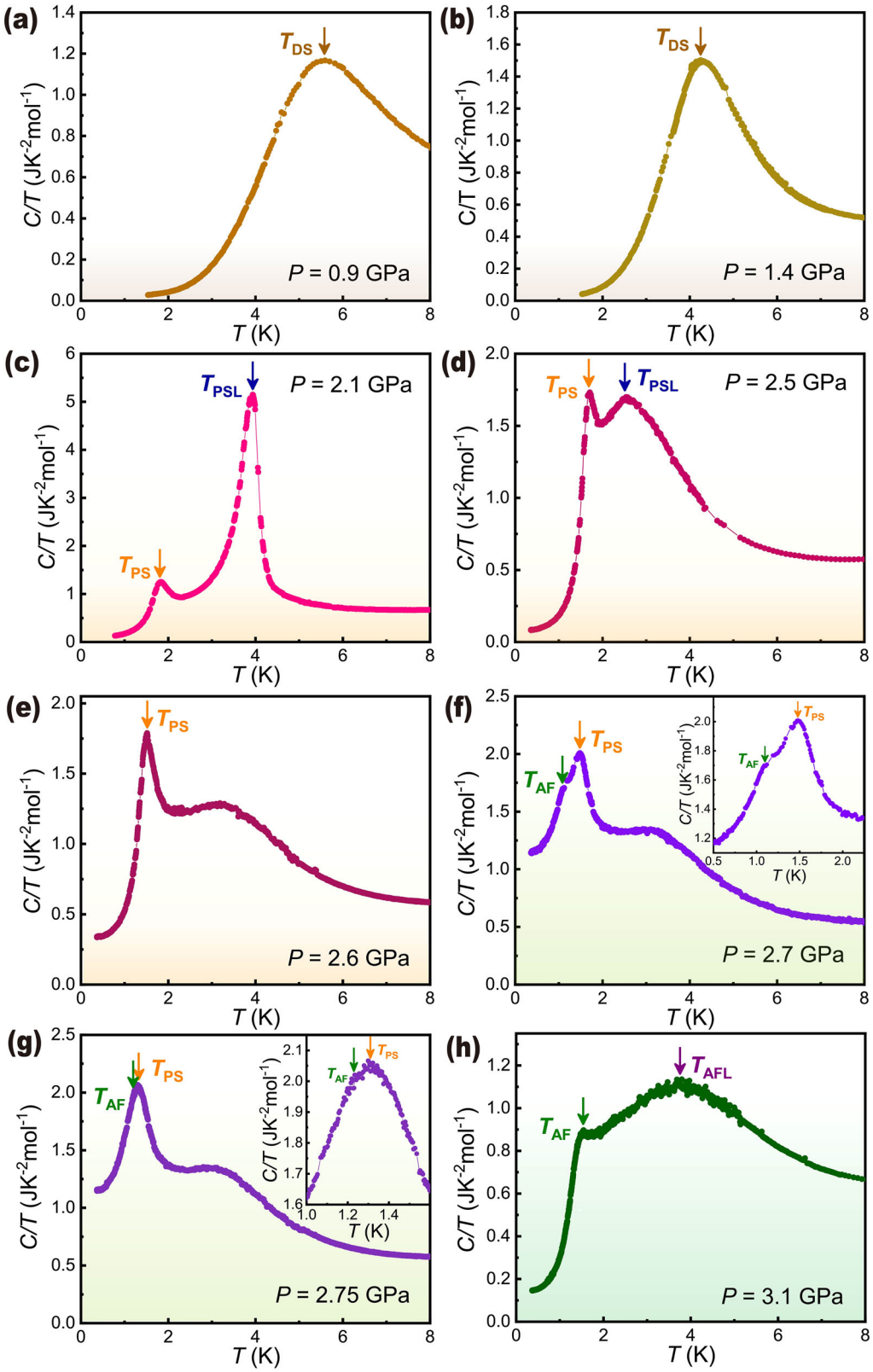

Fig. 2 | The results of temperature (T) dependence of high-pressure heat capacity (*C*) of $SrCu_2(BO_3)_2$. a, **b** are the plots of *C*/*T* versus *T* measured at 0.9 and 1.4 GPa, which show the typical characteristic of the dimmer singlet (DS) phase. The position of the maximum of the hump (T_{DS}) signifies the formation temperature of the DS phase. (**c**–**e** display the pressure-induced two transitions upon cooling measured at 2.1, 2.5, and 2.6 GPa. The high-temperature peak relates to the plaquette-singlet liquid (PSL), while the low-temperature peak is associated with the plaquette-singlet phase (PS). The sharp PSL peak at 2.1 GPa relates to a critical point or a terminal point of phase boundary[39]. **f**, **g** are the results obtained at 2.7 and 2.75 GPa, respectively, illustrating the emergence of the antiferromagnetic (AF) phase. The insets show the transitions at low temperatures for a better view. **h** presents the results of *C*/*T* at 3.1 GPa, exhibiting an AF ground-state below T_{AF} and an anti-ferromagnetic liquid phase below the crossover temperature T_{AFL}.

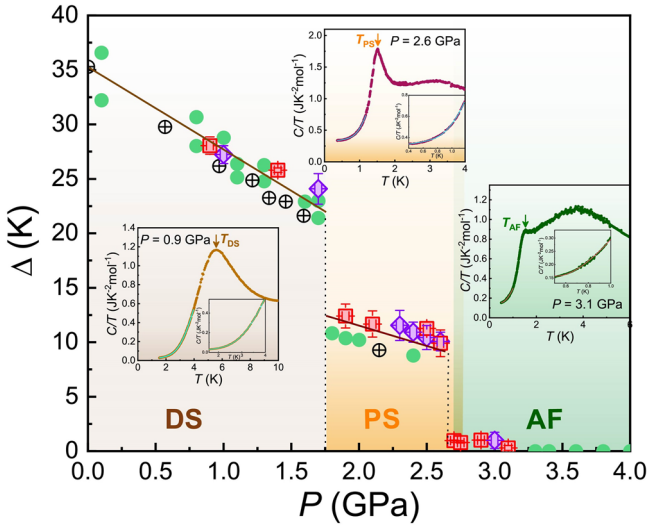

Fig. 3 | Pressure dependence of gap extracted from low-temperature fits to *C*/*T*. The red squares and purple diamonds are the data obtained from this work, and the rest symbols are the data from refs. 37,38. The three insets are the plots of *C*/*T* versus temperature measured at three typical pressures with the fitting details at low temperatures. Here, *C* represents the heat capacity, *T* is the temperature. The error bars associated with the gap reflect a thorough consideration of the fitting ranges and consistency with experimental data. The error bars related to pressure account for the temperature uncertainty in the superconducting transition temperature T_c measured for Pb.

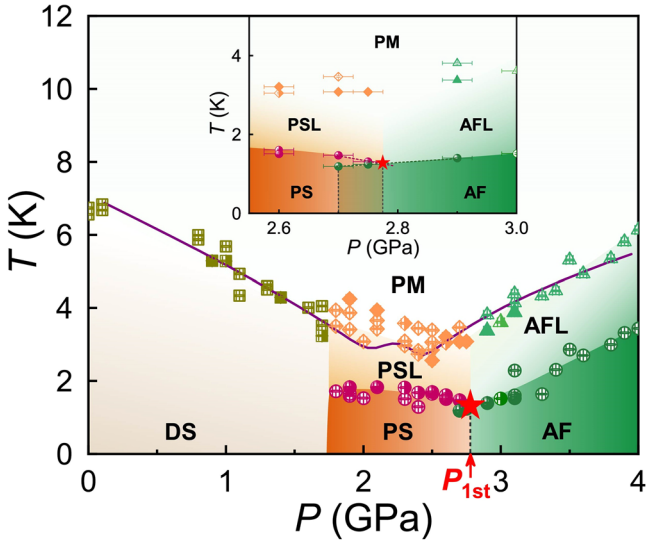

Fig. 4 | The complete *P*-*T* Phase diagram of SrCu2(BO3)2. The acronyms PM, DS, PSL, PS, AFL, and AF stand for paramagnetic, dimer singlet, plaquette-singlet liquid, plaquette-singlet, antiferromagnetic liquid, and antiferromagnetic phases, respectively. P_{1st} represents the pressure of the first-order transition. The solid and half-filled markers are the data obtained from two samples separately in this study, while the hollow ones are the data obtained from our previous study[38], all of which are in good agreement. The error bars related to pressure account for the temperature uncertainty in the superconducting transition temperature T_c measured for Pb. The temperature error is determined based on the accuracy of the temperature sensor. The purple solid line, which goes through the data points of T_{DS}, T_{PSL}, and T_{AFL} (the crossover scale of the AF correlation, denoted by the green triangles), is from an ED calculation on the SS model with functions of $J'(P)$ and $J(P)$ mentioned above[38]. The inset zooms in the transition near the boundary of the PS phase and AF phase. The red star is the critical pressure point of 2.78 GPa, which is determined by an extrapolation of onset temperatures of the PS phase and AF phase (see red and green dash lines).

low-temperature peak is associated with the transition temperature of PSL-PS (T_{PS}). These two states present in the range of 2.1–2.6 GPa (Fig. 2c–e). The sharp PSL peak with significant intensity at 2.1 GPa exhibits characteristics of a critical point (a terminal point of phase boundary)[39], and it broadens and decreases with further compression. At 2.7 GPa, an AF phase appears at a temperature slightly lower than T_{PS} (Fig. 2f). It seems that the three phases, AF, PS, and PSL phases are compatible (Fig. 2f). Such a feature can be observed until 2.75 GPa (Fig. 2g). At 2.9 GPa and above, the PS phase no longer exists (the reason will be discussed below), but the AF phase prevails (Fig. 2h). A hump feature is also observed at the temperature higher than T_{AF}. We define the temperature at the maximum of the hump as the onset temperature of the AF liquid state (T_{AFL}), below which the spins start to establish the effective AF interactions but have not been ordered yet[3]. The true AF long-range order is established below the T_{AF} peak, as shown in Fig. 2h for 3.1 GPa. We reproduce the experimental features with a different sample cut from a different batch (see Supplementary Note 1 and data shown in Supplementary Fig. 3).

The low-temperature data of *C*/*T* are fitted by the form[38]: $C/T = a_0 + a_1T^2 + (a_2/T^3)\exp(-\Delta/T)$, where the first two terms of *C*/*T* account for contributions from electrons and phonons of wire, heater and sample, and the third term from sample's gap. Δ is the activation gap and a_0, a_1, and a_2 fitting parameters. Figure 3 (Supplementary Data 2) shows the extracted gaps (red squares and purple diamonds) along with the counterparts reported previously[37–39], revealing that both DS and PS phases are gaped, being in good agreement with both experimental and theoretical results[37,38,41–43,45,46]. The clear drops in the gap at the boundaries of the DS-PS and PS-AF phase transitions further confirm that these transitions are first-order. Mind that the system may resolve a tiny activation gap due to tiny pressure inhomogeneity or sample impurity in the AF phase. Considering that the values of the tiny gaps are less than the transition temperatures, as shown in Fig. 2, a homogenous and clean system is therefore gapless when $P > 2.7$ GPa. The gapless state is the hallmark of the existence of the AF phase based on the gapless Goldstone modes[57].

Phase diagram

We summarize our experimental results in the phase diagram (Supplementary Data 3 and Fig. 4). All the data shown in the main panel are from heat-capacity measurements, in which the solid and half-filled markers are the data obtained from two samples separately in this study, while the open markers are the results from our previous study[38]. Mind that most error bars are smaller than corresponding makers, except those in the inset. All data measured on the different samples are well consistent with each other. There are three regimes in the phase diagram: below 1.8 GPa, the ground-state of $SrCu_2(BO_3)_2$ holds the DS phase (the left regime); at pressure of about 1.8 GPa, the system enters the PS phase (the middle regime); further compression to about 2.7 GPa, the AF phase sets in and stabilizes up to 4 GPa. To understand the details of the PS-AF phase transition, we zoom in on the phase diagram near the boundary of these two phases as the inset of the main panel. A coexistence of PS and AF phases is observed in a very narrow pressure range. To find the precise pressure point for the PS-AF phase transition, we extrapolate the plot of temperature versus pressure for the two phases near the boundary (see red dash and green dash lines), which gives rise to an intersection located at 2.78 GPa. This intersection, marked by a red star, is defined as the critical pressure for the PS-AF phase transition. It is apparent that at a pressure above 2.78 GPa, the PS phase completely transforms into the AF phase.

We find the transition from the PS phase to the AF phase is not a quantum critical point, but a sudden change from one phase to the other. Moreover, the drop in the gap from the PS phase to the AF phase indicates a jump in the free energy of the system. Those two aspects show that the PS-AF transition in $SrCu_2(BO_3)_2$ is clearly first-order, giving a decisive answer on how the lattice translation symmetry-breaking PS phase evolves into the spin rational symmetry-breaking AF phase. Such a scenario can also be supported by the plots of heat capacity versus temperature measured at 2.7 GPa and 2.75 GPa (Fig. 2f, g), where the *C*/*T* (*T*) at T_{AF} is getting higher than that at T_{PS} as the pressure approaches the AF regime. These changes are in concordance with the well-known behavior of a first-order transition.

It is worth noting that the observation of the narrow overlap of the PS and AF phases should come from the tiny inhomogeneity of the pressure because $SrCu_2(BO_3)_2$ is a pressure-sensitive material[58–60]. A slight difference in the pressure environment (the pressure at the center and the edges of the sample) may influence the detected critical points of the two-phase transitions. Fortunately, this by-product provides us a way to determine the critical pressure/temperature point of the PS-AF transition, which meets at nearly the same pressure/temperature point defined as the bi-critical point in the phase transition theory. The observation of the bi-critical transition between PSL-PS and AFL-AF phases in $SrCu_2(BO_3)_2$ is reminiscent of what has been observed in the Fe-based superconductor $Ca_{0.73}La_{0.27}FeAs_2$[58], in which the sample undergoes a first-order transition from the AF phase to a superconducting (SC) phase, accompanied by PM-AF and PM-SC transitions at a bi-critical point. Another similar observation has also been made in a heavy-fermion compound, YbAgGe[61].

Discussion

The observation of the pressure-induced first-order transition between the plaquette-singlet phase and the antiferromagnetic phase in $SrCu_2(BO_3)_2$ delivers a clear message that the previously proposed DQCP is lost in this pressurized material. In the recent theoretical developments of several important DQCP lattice models, both quantum spin models[25–28] and interacting Dirac fermion models with Kane-Mele and plaquette interactions[28,35], one consistently finds that the seemingly continuous transitions therein, irrespective of VBS to AF phases, or from quantum spin Hall (QSH) to SC phases, where both sides are spontaneously symmetry-breaking phases and the transitions are tuned by a single parameter, cannot be compatible with more fundamentally "first-principle" tests as continuous transitions with CFT description. These tests include the conformal bootstrap bounds of critical exponents for emergent continuous symmetry and the positivity requirement of the entanglement entropy[24–36,62]. The messages from these analyses imply that the DQCPs with their present lattice model realizations are either first-order transitions or some other more complicate scenarios, such as multicritical points and complex fixed points, which now one does not have a completely controlled theoretical framework to calculate their precise properties[16,23,62].

Our experimental results in this study, therefore, come as a great relief that the PS-AF transition in pressurized $SrCu_2(BO_3)_2$ at zero field is first-order, putting the vital and final piece of the puzzle onto the phase diagram and clarifying the two-decade-long debates on DQCPs of $SrCu_2(BO_3)_2$ and related models. Our results also resonate nicely with the recent quantum entanglement understanding that the proposed DQCPs in 2D quantum spin or interacting Dirac fermion models are eventually first-order transitions[25–36].

Besides, another interesting observation in this study is that the C/T data measured at very low temperature (roughly the a_0 in the gap fitting function) exhibits an enhanced value at the temperature around the bi-critical point (see Supplementary Note 2 and date shown in Supplementary Fig. 4). This might suggest there exist enhanced fluctuations in the vicinity of the bi-critical point and might imply that, if one could further suppress the bi-critical point by competing interactions or geometry frustrations, a DQCP or even the speculated quantum spin liquid state separating the PS and AF phases[54–56] could emerge. Similar behavior has been observed in the bi-critical point of heavy-fermion compound YbAgGe[61] with the specific heat, the Grüneisen parameter, and the magnetocaloric effect. It is certainly of significance to carry out the comparison on $SrCu_2(BO_3)_2$ and $Ca_{0.73}La_{0.27}FeAs_2$ by distinguishing the commonness and peculiarity and finding clues to understand the superconductivity in the proximity of the AF phase. It is expected that our results will provide valuable experimental foundations and theoretical inspirations for eventually extending the paradigm of quantum phase transitions beyond Landau-Ginzberg-Wilson.

Methods

High-pressure heat-capacity measurements

In this study, a piston/cylinder-type high-pressure cell was employed for the heat-capacity measurements up to ~3.2 GPa, as shown in Supplementary Fig. 1. This high-pressure cell is integrated with our low-temperature and high magnetic field systems, which allows us to cool the compressed sample as low as 0.33 K with a magnetic field up to 14 T. Single-crystal $SrCu_2(BO_3)_2$ samples with dimensions of about 1.1 × 1.5 × 0.17 mm and 0.9 × 1.0 × 0.15 mm were used for the two independent measurements, respectively. Constantan, a convenient material with a weak temperature dependence in resistivity, whose total change in resistance over the temperature range of measurements was 5%[63,64], was used as the heater. In the experiments, we glued the constantan to one side of the sample. The room temperature resistance (R) of the heater was determined by measuring its length under a microscope and using the known resistance per unit length of our wire, which was measured separately. Platinum wires with a diameter of 25 μm were spot-welded to the ends of the heater. A chromel-AuFe (0.07%) thermocouple was fixed on the other side of the sample. Subsequently, the sample, together with a piece of Pb used for the pressure determination of the sample was loaded into a Teflon capsule filled with the liquid of glycerin/water (3:2) in order to maintain the sample in a stable hydrostatic pressure environment within the pressure range up to 5 GPa[65]. Previous research on the hydrostatic homogeneity of this pressure-transmitting medium has indicated that the standard deviation of pressure below 3 GPa is less than 0.01 GPa[65]. Taking into account the temperature error of T_c for measuring Pb, the overall measured pressure error in the pressure range investigated is within 0.05 GPa.

During the measurements, we applied a sinusoidal alternative current (AC) excitation I with a frequency f to the heater. The resulting temperature oscillations ΔT in the sample with a frequency of $2f$ were detected by the thermocouple, which is amplified by an SR554 preamplifier and then measured by an SR830 lock-in amplifier[66,67]. This approach allows us to retrieve the sample's heat-capacity value by converting the heater's modest temperature oscillation into an AC voltage signal. Knowing input power (P, $P = I^2R$), we can calculate the value of $P/(f\Delta T)$, which directly relates to the heat capacity at the optimal measurement frequency[66,67].

During the cooling process, adjustments were made to the optimal frequency of the ac-power input to ensure necessary quasi-adiabatic conditions, which are essential for accurate calorimetric measurements[68]. Further details on the principles and methodologies used in the high-pressure heat-capacity measurements can be found in the Supplementary Note 2. Moreover, we adopted the relationship between the thermocouple's Seebeck coefficient and temperature at ambient pressure since the pressure effect on the thermocouples is ignored, which is experimentally found very small[69,70]. The contribution of the glycerin-water pressure-transmitting medium was estimated based on the observed reduction in specific heat (μJ K^{-1}) at the glass transition during cooling. To isolate the effect of the medium surrounding the sample, separate experiments were performed using only the liquid in the pressure cell. A map of $C(P,T)$ for the glycerin-water mixture was generated, enabling us to estimate its contribution to the overall heat-capacity measurements.

Data availability

The data shown in Figs. 2–4 can be accessed in the online version of this paper and its supplementary information files. Additional data supporting the findings of this study can be obtained from the corresponding authors upon request.

Received: 5 November 2024; Accepted: 23 January 2025;
Published online: 22 February 2025

References

1. Senthil, T., Vishwanath, A., Balents, L., Sachdev, S. & Fisher, M. P. Deconfined quantum critical points. *Science* **303**, 1490–1494 (2004).
2. Senthil, T., Balents, L., Sachdev, S., Vishwanath, A. & Fisher, M. P. A. Quantum criticality beyond the Landau-Ginzburg-Wilson paradigm. *Phys. Rev. B* **70**, 144407 (2004).
3. Landau, L. D., Lifshitz, E. M. & Pitaevskii, L. P. *Statistical Physics*. chap. XIV, P446 (Butterworth-Heinemann, 1980).
4. Wilson, K. G. The renormalization group and critical phenomena. *Rev. Mod. Phys.* **55**, 583–600 (1983).

5. Sachdev, S. *Quantum Phase Transitions* (Cambridge University Press, 2001).
6. Berezinskii, V. Destruction of long-range order in one-dimensional and two-dimensional systems having a continuous symmetry group 1. Classical systems. *Sov. Phys. JETP* **32**, 493–500 (1971).
7. Kosterlitz, J. M. & Thouless, D. J. Ordering, metastability and phase transitions in two-dimensional systems. *J. Phys. C Solid State Phys.* **6**, 1181–1203 (1973).
8. Barkeshli, M. & Wen, X.-G. Phase transitions in Zn gauge theory and twisted Zn topological phases. *Phys. Rev. Lett.* **105**, 216804 (2010).
9. Wen, X.-G. Colloquium: zoo of quantum-topological phases of matter. *Rev. Mod. Phys.* **89**, 041004 (2017).
10. Sandvik, A. W. Evidence for deconfined quantum criticality in a two-dimensional Heisenberg model with four-spin interactions. *Phys. Rev. Lett.* **98**, 227202 (2007).
11. Lou, J., Sandvik, A. W. & Kawashima, N. Antiferromagnetic to valence-bond-solid transitions in two-dimensional SU(*N*) Heisenberg models with multispin interactions. *Phys. Rev. B* **80**, 180414 (2009).
12. Block, M. S., Melko, R. G. & Kaul, R. K. Fate of CP$N-1$ fixed points with q monopoles. *Phys. Rev. Lett.* **111**, 137202 (2013).
13. Nahum, A., Chalker, J. T., Serna, P., Ortuño, M. & Somoza, A. M. Deconfined quantum criticality, scaling violations, and classical loop models. *Phys. Rev. X* **5**, 041048 (2015).
14. Nahum, A., Serna, P., Chalker, J. T., Ortuño, M. & Somoza, A. M. Emergent SO(5) symmetry at the Néel to valence-bond-solid transition. *Phys. Rev. Lett.* **115**, 267203 (2015).
15. Shao, H., Guo, W. & Sandvik, A. W. Quantum criticality with two length scales. *Science* **352**, 213–216 (2016).
16. Wang, C., Nahum, A., Metlitski, M. A., Xu, C. & Senthil, T. Deconfined quantum critical points: symmetries and dualities. *Phys. Rev. X* **7**, 031051 (2017).
17. Qin, Y. Q. et al. Duality between the deconfined quantum-critical point and the bosonic topological transition. *Phys. Rev. X* **7**, 031052 (2017).
18. Ma, N. et al. Dynamical signature of fractionalization at a deconfined quantum critical point. *Phys. Rev. B* **98**, 174421 (2018).
19. Ma, N., You, Y.-Z. & Meng, Z. Y. Role of Noether's theorem at the deconfined quantum critical point. *Phys. Rev. Lett.* **122**, 175701 (2019).
20. Zhao, B., Takahashi, J. & Sandvik, A. W. Multicritical deconfined quantum criticality and Lifshitz point of a helical valence-bond phase. *Phys. Rev. Lett.* **125**, 257204 (2020).
21. Da Liao, Y., Xu, X. Y., Meng, Z. Y. & Qi, Y. Dirac fermions with plaquette interactions. III. SU(*N*) phase diagram with Gross-Neveu criticality and first-order phase transition. *Phys. Rev. B* **106**, 075111 (2022).
22. Liu, Y. et al. Superconductivity from the condensation of topological defects in a quantum spin-Hall insulator. *Nat. Commun.* **10**, 2658 (2019).
23. Nahum, A. Note on Wess-Zumino-Witten models and quasiuniversality in $2+1$ dimensions. *Phys. Rev. B* **102**, 201116 (2020).
24. Poland, D., Rychkov, S. & Vichi, A. The conformal bootstrap: theory, numerical techniques, and applications. *Rev. Mod. Phys.* **91**, 015002 (2019).
25. Wang, Y.-C., Ma, N., Cheng, M. & Meng, Z. Y. Scaling of the disorder operator at deconfined quantum criticality. *SciPost Phys.* **13**, 123 (2022).
26. Zhao, J., Wang, Y.-C., Yan, Z., Cheng, M. & Meng, Z. Y. Scaling of entanglement entropy at deconfined quantum criticality. *Phys. Rev. Lett.* **128**, 010601 (2022).
27. Song, M. et al. Evolution of entanglement entropy at SU(N) deconfined quantum critical points. Preprint at https://arxiv.org/abs/2307.02547 (2023).
28. Liu, Z. H. et al. Fermion disorder operator at Gross-Neveu and deconfined quantum criticalities. *Phys. Rev. Lett.* **130**, 266501 (2023).
29. Chester, S. M. & Su, N. Bootstrapping deconfined quantum tricriticality. *Phys. Rev. Lett.* **132**, 111601 (2024).
30. Song, M. H., Zhao, J. R., Meng, Z. Y., Xu, C. K. & Cheng, M. Extracting subleading corrections in entanglement entropy at quantum phase transitions. *SciPost Phys.* **17**, 010 (2024).
31. D'Emidio, J. et al. Diagnosing weakly first-order phase transitions by coupling to order parameters. *SciPost Phys.* **15**, 061 (2023).
32. Deng, Z., Liu, L., Guo, W. & Lin, H.-Q. Diagnosing quantum phase transition order and deconfined criticality via entanglement entropy. *Phys. Rev. Lett.* **133**, 100402 (2024).
33. Chen, B. B., Zhang, X., Wang, Y. X., Sun, K. & Meng, Z. Y. Phases of $(2+1)$D SO(5) non-linear sigma model with a topological term on a sphere: multicritical point and disorder phase. *Phys. Rev. Lett.* **132**, 246503 (2024).
34. Takahashi, J., Shao, H., Zhao, B. W., Guo, W. & Sandvik, A. W. SO(5) multicriticality in two-dimensional quantum magnets. Preprint at https://arxiv.org/abs/2405.06607 (2024).
35. Da Liao, Y., Pan, G., Jiang, W., Qi, Y. & Meng, Z. Y. The teaching from entanglement: 2D SU(2) antiferromagnet to valence bond solid deconfined quantum critical points are not conformal. Preprint at https://arxiv.org/abs/2302.11742 (2023).
36. Liu, Z. H. et al. Disorder operator and Renyi entanglement entropy of symmetric mass generation. *Phys. Rev. Lett.* **132**, 156503 (2024).
37. Zayed, M. et al. 4-spin plaquette singlet state in the Shastry–Sutherland compound $SrCu_2(BO_3)_2$. *Nat. Phys.* **13**, 962–966 (2017).
38. Guo, J. et al. Quantum phases of $SrCu_2(BO_3)_2$ from high-pressure thermodynamics. *Phys. Rev. Lett.* **124**, 206602 (2020).
39. Jiménez, J. L. et al. A quantum magnetic analogue to the critical point of water. *Nature* **592**, 370–375 (2021).
40. Cui, Y. et al. Proximate deconfined quantum critical point in $SrCu_2(BO_3)_2$. *Science* **380**, 1179–1184 (2023).
41. Kageyama, H. et al. Specific heat study of $SrCu_2(BO_3)_2$. *Phys. B Condens. Matter* **281**, 667–668 (2000).
42. Koga, A. & Kawakami, N. Quantum phase transitions in the Shastry-Sutherland model for $SrCu_2(BO_3)_2$. *Phys. Rev. Lett.* **84**, 4461 (2000).
43. Kageyama, H. et al. Exact dimer ground state and quantized magnetization plateaus in the two-dimensional spin system $SrCu_2(BO_3)_2$. *Phys. Rev. Lett.* **82**, 3168 (1999).
44. Smith, R. W. & Keszler, D. A. Synthesis, structure, and properties of the orthoborate $SrCu_2(BO_3)_2$. *J. Solid State Chem.* **93**, 430–435 (1991).
45. Waki, T. et al. A novel ordered phase in $SrCu_2(BO_3)_2$ under high pressure. *J. Phys. Soc. Jpn.* **76**, 073710 (2007).
46. Takigawa, M., Waki, T., Horvatić, M. & Berthier, C. Novel ordered phases in the orthogonal dimer spin system $SrCu_2(BO_3)_2$. *J. Phys. Soc. Jpn.* **79**, 011005 (2010).
47. Shastry, B. S. & Sutherland, B. Exact ground state of a quantum mechanical antiferromagnet. *Phys. B + C* **108**, 1069 (1981).
48. Corboz, P. & Mila, F. Tensor network study of the Shastry-Sutherland model in zero magnetic field. *Phys. Rev. B* **87**, 115144 (2013).
49. Albrecht, M. & Mila, F. First-order transition between magnetic order and valence bond order in a 2D frustrated Heisenberg model. *Europhys. Lett.* **34**, 145–150 (1996).
50. Miyahara, S. & Ueda, K. Exact dimer ground state of the two dimensional Heisenberg spin system $SrCu_2(BO_3)_2$. *Phys. Rev. Lett.* **82**, 3701 (1999).
51. Müller-Hartmann, E., Singh, R. R. P., Knetter, C. & Uhrig, G. S. Exact demonstration of magnetization plateaus and first-order Dimer-Néel phase transitions in a modified Shastry-Sutherland model for $SrCu_2(BO_3)_2$. *Phys. Rev. Lett.* **84**, 1808 (2000).
52. Boos, C. et al. Competition between intermediate plaquette phases in $SrCu_2(BO_3)_2$ under pressure. *Phys. Rev. B* **100**, 140413 (2019).
53. Xi, N., Chen, H., Xie, Z. Y. & Yu, R. Plaquette valence bond solid to antiferromagnet transition and deconfined quantum critical point of the Shastry-Sutherland model. *Phys. Rev. B* **107**, L220408 (2023).
54. Wang, L. & Sandvik, A. W. Critical level crossings and gapless spin liquid in the square-lattice spin-1/2 J_1-J_2 Heisenberg antiferromagnet. *Phys. Rev. Lett.* **121**, 107202 (2018).
55. Liu, W.-Y. et al. Gapless quantum spin liquid and global phase diagram of the spin-1/2 J_1-J_2 square antiferromagnetic Heisenberg model. *Sci. Bull.* **67**, 1034–1041 (2022).

56. Yang, J., Sandvik, A. W. & Wang, L. Quantum criticality and spin liquid phase in the Shastry-Sutherland model. *Phys. Rev. B* **105**, L060409 (2022).
57. Goldstone, J., Salam, A. & Weinberg, S. Broken symmetries. *Phys. Rev.* **127**, 965 (1962).
58. Zhou, Y. Z. et al. Observation of a bi-critical point between antiferromagnetic and superconducting phases in pressurized single crystal $Ca_{0.73}La_{0.27}FeAs_2$. *Sci. Bull.* **62**, 857–862 (2017).
59. Wang, P. Y. et al. Pressure-induced dependence of transport properties and lattice stability of $CaK(Fe_{1-x}Ni_x)_4As_4$ (x=0.04 and 0) superconductors with and without a spin-vortex crystal state. *Phys. Rev. B* **108**, 054415 (2023).
60. Yang, C. et al. Quasi-uniaxial pressure induced superconductivity in the stoichiometric compound UTe_2. *Phys. Rev. B* **106**, 024503 (2022).
61. Tokiwa, Y., Garst, M., Gegenwart, P., Bud'ko, S. L. & Canfield, P. C. Quantum bicriticality in the heavy-fermion metamagnet YbAgGe. *Phys. Rev. Lett.* **111**, 116401 (2013).
62. Nakayama, Y. & Ohtsuki, T. Necessary condition for emergent symmetry from the conformal bootstrap. *Phys. Rev. Lett.* **117**, 131601 (2016).
63. Furukawa, G. T., Reilly, M. L. & Saba, W. G. Electrical resistances of wires of low temperature coefficient of resistance useful in calorimetry (10°–380°K). *Rev. Sci. Instrum.* **35**, 113–114 (1964).
64. Lee, H. et al. Pressure-induced superconducting state of antiferromagnetic $CaFe_2As_2$. *Phys. Rev. B* **80**, 024519 (2009).
65. Klotz, S., Takemura, K., Strässle, T. & Hansen, T. Freezing of glycerol–water mixtures under pressure. *J. Phys. Condens. Matter* **24**, 325103 (2012).
66. Eichler, A. & Gey, W. Method for the determination of the specific heat of metals at low temperatures under high pressures. *Rev. Sci. Instrum.* **50**, 1445–1452 (1979).
67. Sidorov, V. A., Thompson, J. & Fisk, Z. Magnetic transitions in a heavy-fermion antiferromagnet U_2Zn_{17} at high pressure. *J. Phys. Condens. Matter* **22**, 406002 (2010).
68. Sullivan, PaulF. & Seidel, G. Steady-state, ac-temperature calorimetry. *Phys. Rev.* **173**, 679 (1968).
69. Jo, Y. J. et al. Refinement of the pressure-temperature phase diagram of the organic superconductor with asymmetric anions (TMTSF) 2FSO3. *Phys. Rev. B* **67**, 014516 (2003).
70. Blatt, F. J., Schroeder, P. A., Foiles, C. L. & Greig, D. *Thermoelectric Power of Metals* (Plenum Press, New York, 1976).

Acknowledgements

This work was supported by the National Key Research and Development Program of China (Grant No. 2021YFA1401800, 2022YFA1403900, No. 2022YFA1403400, and No. 2021YFA1400400), the NSF of China (Grant Numbers Grants No. U2032214, 12122414, 12104487 and 12004419), and the Strategic Priority Research Program (B) of the Chinese Academy of Sciences (Grant No. XDB25000000 and No. XDB33000000), the K. C. Wong Education Foundation (GJTD-2020-01). J. G. and S. C. are grateful for support from the Youth Innovation Promotion Association of the CAS (2019008) and the China Postdoctoral Science Foundation (E0BK111). C. H. and Z. Y. M. acknowledge the support from the Research Grants Council (RGC) of Hong Kong Special Administrative Region (SAR) (Projects Nos. 17301721, AoE/P-701/20, 17309822 and C7037-22GF, 17302223, 17301924), the ANR/RGC Joint Research Scheme sponsored by the RGC of Hong Kong SAR of China and French National Research Agency (Project No. A HKU703/22) and the HKU Seed Funding for Strategic Interdisciplinary Research "Many-body paradigm in quantum moiré material research". We thank the HPC2021 system under the Information Technology Services, University of Hong Kong, as well as the Beijing PARATERA Tech CO., Ltd. (URL: https://cloud.paratera.com) for providing HPC resources that have contributed to the research results reported within this paper.

Author contributions

Z.Y.M., L.L.S., and J.G. initiated the work. L.L.S., Z.Y.M. supervised the project. W.S.H and S.L.L. grew the $SrCu_2(BO_3)_2$ single crystals. J.G. and P.Y.W. conducted the high-pressure heat-capacity measurements with the help of S.C., J.Y.Z, J.Y.H., X.T.C., and Y.Z.Z. L.L.S., Z.Y.M., J.G., C.H., and Q.W. carried out the data analysis. Z.Y.M., L.L.S., Q.W., J.G., and C.H. wrote the manuscript with the efforts of all authors.

Competing interests

Professor Liling Sun is serving as an Editorial Board/Guest Member (EBM) for *Communications Physics*. All other authors declare no competing interests.

Additional information

Supplementary information The online version contains supplementary material available at https://doi.org/10.1038/s42005-025-01976-8.

Correspondence and requests for materials should be addressed to Zi Yang Meng or Liling Sun.

Peer review information *Communications Physics* thanks the anonymous reviewers for their contribution to the peer review of this work.